Supplementary material

S1. Aerosol reference data comparison

We validate the capabilities of the CESM experiments in simulating specific and bulk aerosol properties against various datasets. Here, "bulk" refers to AOD contributions from all aerosols (sulfate + BC + dust + ammonium + organics + sea salt + nitrates).

S1.1 MODIS

We compare the control simulations against a level-3 1^o monthly-gridded product from the moderate resolution imaging spectroradiometer (MODIS) collection-6 suite, retrieved from MODIS Terra and available at https://ladsweb.nascom.nasa.gov/api/v1/productPage/product=MOD08_M3. We make use of 14-year AOD averages from 2001 – 2014 (Platnick et al., 2015). The label "level-3" (L3) refers to the datasets being monthly statistical summaries of bulk AOD that combine multiple satellite passes into a global dataset at monthly intervals. Specifically, this product contains over 700 derived variables such as atmospheric optical properties, ozone burden, atmospheric water vapor, cloud optical and physical properties, and atmospheric stability parameters. The retrieval algorithm for 550nm AOD makes use of a merged dark target and deep blue algorithm. The algorithm is suitable for this study due to the high spatial variability of vegetation and brightness factor across the TP region and the rest of south Asia.

Aerosol properties are only retrieved by Terra under clear sky conditions, so the L3 gridcells are only filled when the number of monthly cloud-free pixels within a 1^ox1^o cell exceeds 6. Since MODIS orbits ~15 times per day, and cloud cover is continually varying, different numbers of pixels go into each 1^o gridcell AOD calculation. The selection of these pixels is based on algorithms that rely on the surface characterization, aerosol model, quality checks, and cloud masking. These algorithms contribute to an expected error for MODIS AOD measurements of $\pm$ $(0.05 + 0.15 \times AOD_{AERONET})$ over land and $\pm(0.04 + 0.1 \times AOD_{AERONET})$ over oceanic regions compared to surface-based observations from AERONET (Levy et al., 2013). Uncertainties in observed AOD specific to certain regions are also noted in Levy et al. (2013), as retrieval processing algorithms vary depending on surface albedo and other regional properties.

S1.2 MISR

Simulated bulk AOD is compared against monthly multi-angle imaging spectroradiometer (MISR) L3 AOD measurements (available at https://l0dup05.larc.nasa.gov/MISR/cgi-bin/MISR/main.cgi) that are binned onto a 0.5^o grid and averaged over a 13-year period from 2002 through 2014 (MISR Science team 2015). MISR is mounted aboard the MODIS Terra satellite, and data products from MISR include surface albedo properties, vegetative indices, and global radiance information. Specifically, AOD is derived for aerosols of differing sizes in blue (443 nm), green (555 nm), red (670 nm), and infrared (865 nm) channels. For this study, we utilize MISR's retrieved bulk AOD in the green (555nm) channel.

Similar to MODIS AOD retrievals, MISR has to contend with uncertainties resulting from cloud contamination, false aerosol detection, and algorithm inadequacies (Witek et al., 2018). Singh et al. (2016) found that the root mean square error (RMSE) between MISR and AERONET AOD to be slightly lower (0.11 – 0.20) than the RMSE between MODIS and AERONET AOD (0.15 – 0.27) across the Indo Gangetic Plain (IGP). More generally, Kahn et al. (2010) reported that MISR AOD retrievals fall within 0.05 or 20% of AERONET-measured AOD values.

S1.3 MACv2

MACv2 AOD estimates were derived as data from AERONET were merged onto background maps from global models that participated in the aerosol model intercomparison (AeroCom) project, effectively making MACv2 an aerosol reanalysis dataset. Data from the maritime aerosol network (MAN) are also included in this version of MAC (Smirnov et al., 2009). The aerosol plumes in this dataset are designed to fit the distribution of mid-visible AOD for the year 2005.

S1.4 MERRA-2

MERRA-2 makes use of global reanalysis to assimilate aerosol observations towards the aim of simulating their interactions with physical atmospheric processes in the climate system. MERRA-2 data can be accessed at: https://gmao.gsfc.nasa.gov/reanalysis/MERRA-2/.

S1.5 AOD validation

Globally averaged, CONT-vr and CONT-un simulate annual AOD values of 0.120 and 0.133, respectively. MODIS and MISR AOD values of 0.172 and 0.148 are observed, respectively, making CONT-un closer to MISR and MODIS observations. MACv2 estimates a global AOD of 0.122, a value more similar to the CESM experiments and less than is observed by satellites. Finally, MERRA-2 estimates a global AOD of 0.141, a value more similar to satellite observations. While both CESM simulations reasonably capture the global annually averaged AOD compared to satellite observations, they do not capture the generally larger annual AOD values in the region bounded by 0^{o}N-60^{o}N and 60^{o}E-140^{o}E.

CONT-un is better correlated with AERONET AOD than CONT-vr, simulating a Pearson correlation (r) value of 0.451, 0.503, and 0.672 for the total, fine-mode, and coarse-mode AOD, respectively, while CONT-vr simulates r- values of 0.335, 0.497, and 0.467. This means that, although the CESM experiments simulate similar mean biases compared to AERONET, the nature of the AOD bias (high or low) changes from site to site between the UN and VR experiments.

Focusing on bulk AOD seasonality across northern India, CONT-vr and CONT-un r-values of 0.716 and 0.715, respectively are calculated against AERONET, while MODIS and MISR are characterized by r-values of 0.825 and 0.886 against AERONET, respectively. Finally, for both the 18- and 57-site average, MACv2 shows the poorest correlations with AERONET with r-values of 0.615 and 0.519, respectively.

Figures

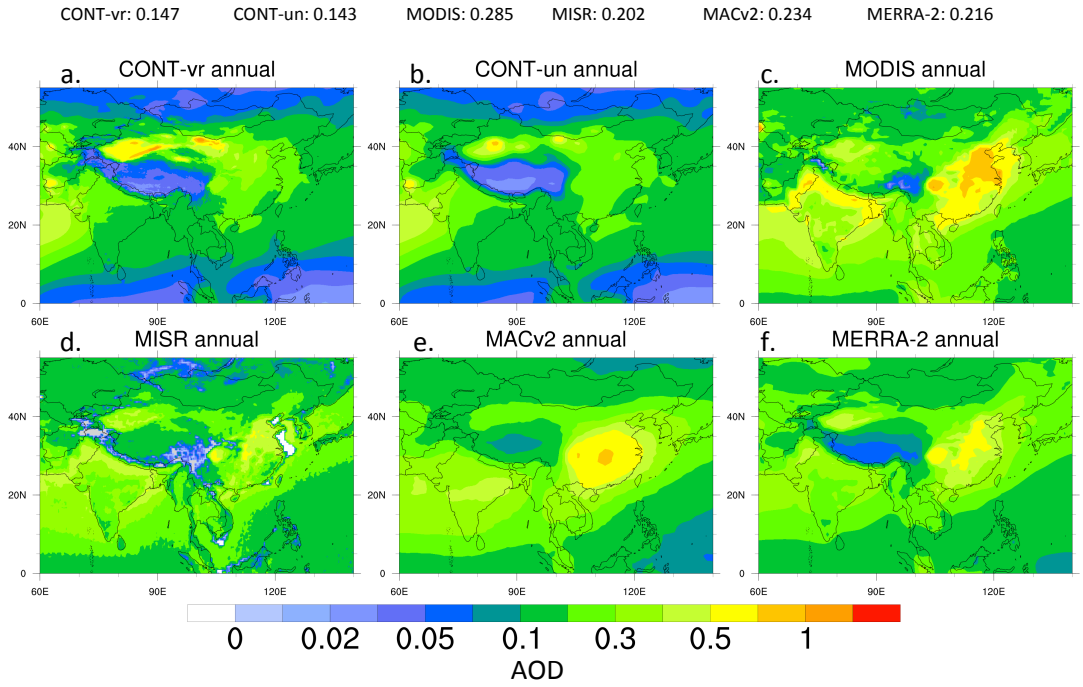

Figure S1. Panels (a), (b), (c), (d), (e), and (f) depict annually averaged AOD values across south-Asia for CONT-vr, CONT-un, MODIS, MISR, MACv2, and MERRA-2, respectively. AOD averages from these respective data between 0°N-60°N and 60°E-140°E are given at the top.

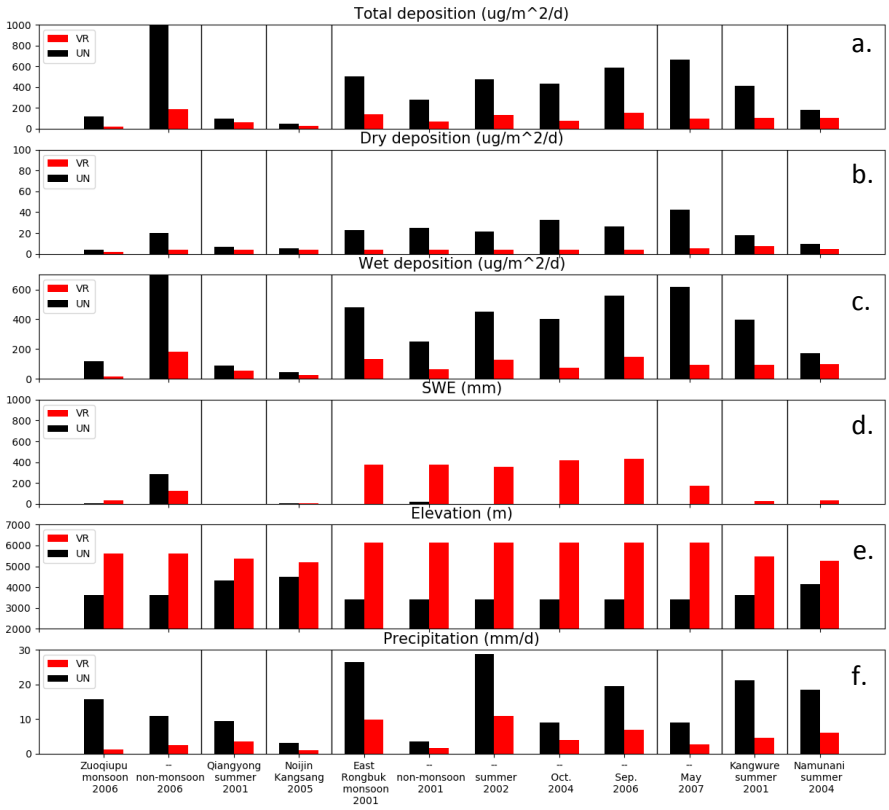

Figure S2. Bar charts at various sites across the Himalaya Mountains discussed in H2014 for (a) total BC deposition, (b) dry BC deposition, (c) wet BC deposition, (d) SWE, (e) elevation, and (f) total precipitation for CONT-vr (red) and CONT-un (black).

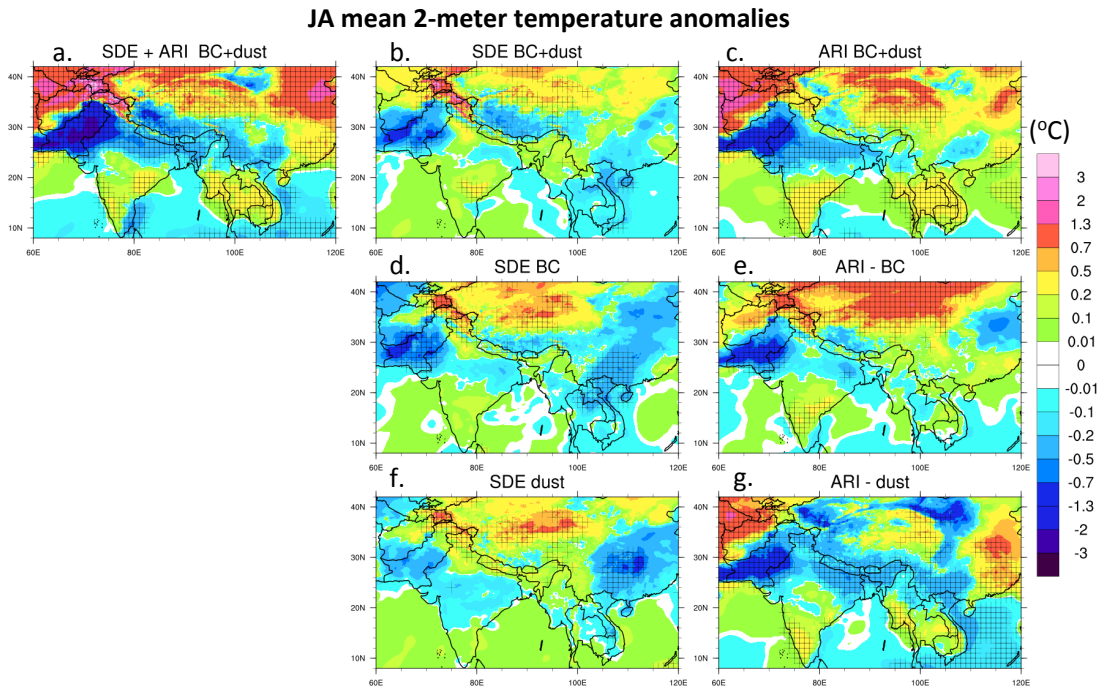

Figure S3. July and August (JA) mean 2-meter temperature (T2) anomalies due to: (a) BCD-induced SDE+ARI, (b) BCD-induced SDE, (c) BCD-induced ARI, (d) BC-induced SDE, (e) BC-induced ARI, (f) dust-induced SDE, and (g) dust-induced ARI. Hatching marks denote areas with *t*-values of 0.9 and greater. It should be kept in mind that, inside the 1^{0} zone, there might be as many as 64 grid points that are characterized by statistically significant values.

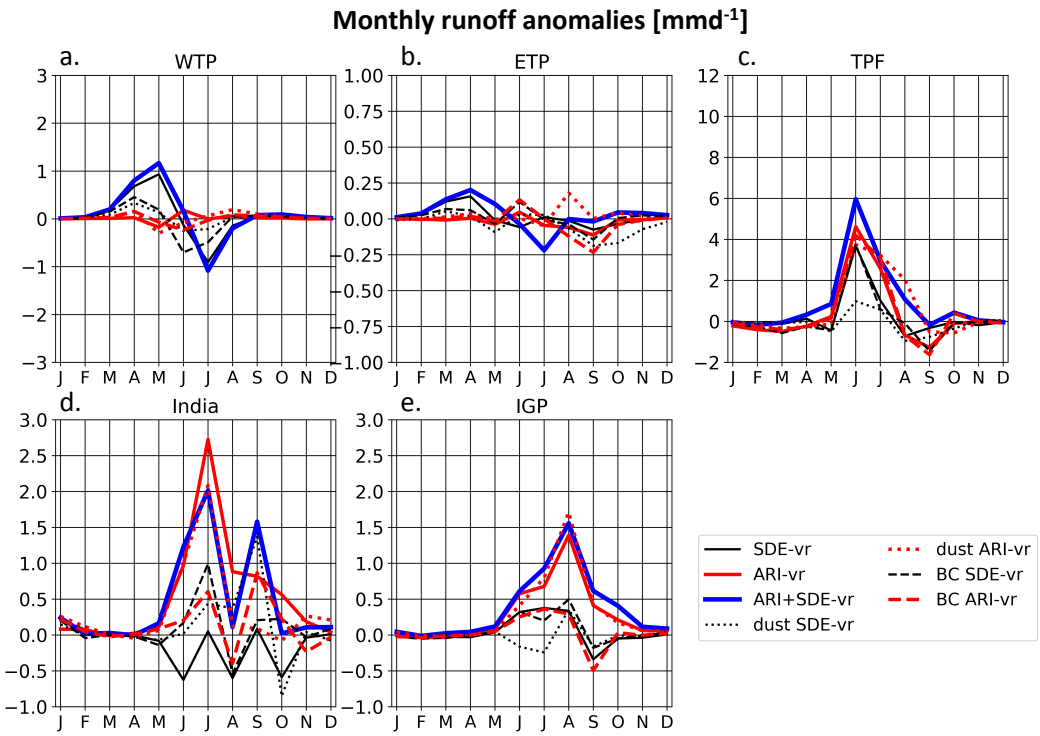

Figure S4. Monthly time series of runoff changes mm d^{-1} due to BCD effects across (a) WTP, (b) the ETP, (c) TPF, (d) India, and (e) IGP.

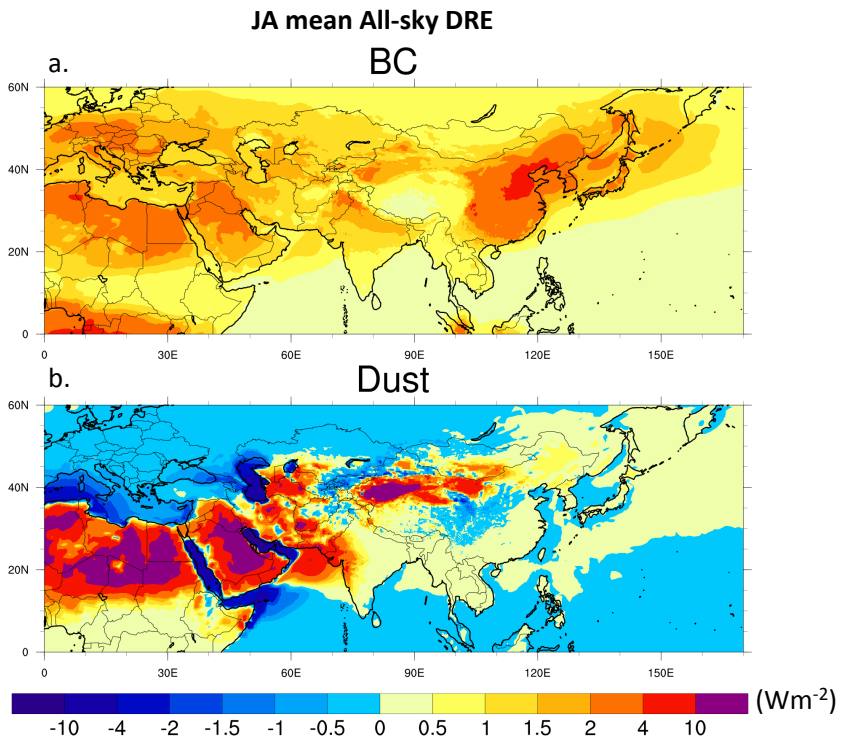

Figure S5. Diagnostically-computed direct radiative effect (DRE) for (a) BC and, (b) dust during JA.

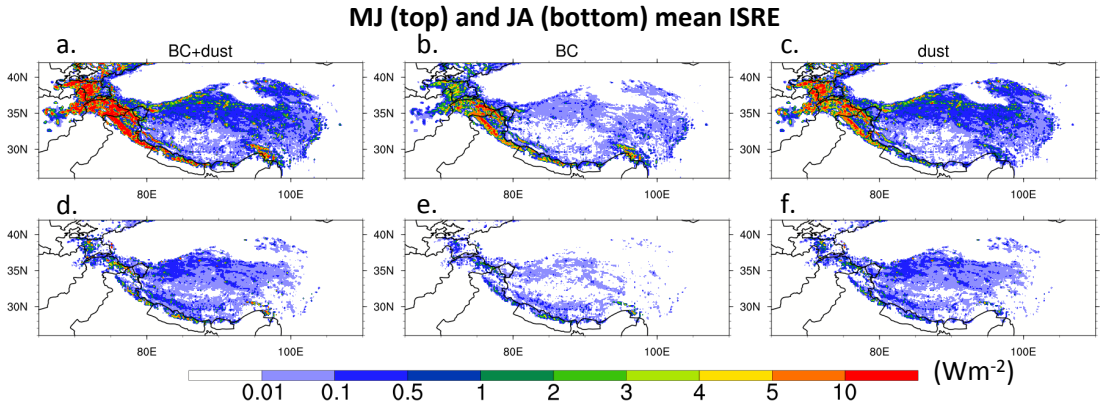

Figure S6. In-snow radiative effect (ISRE) during averaged during MJ for (a) BC+dust, (b) BC, and (c) dust. Panels (d), (e), and (f) are the same as (a)-(c) but for JA.

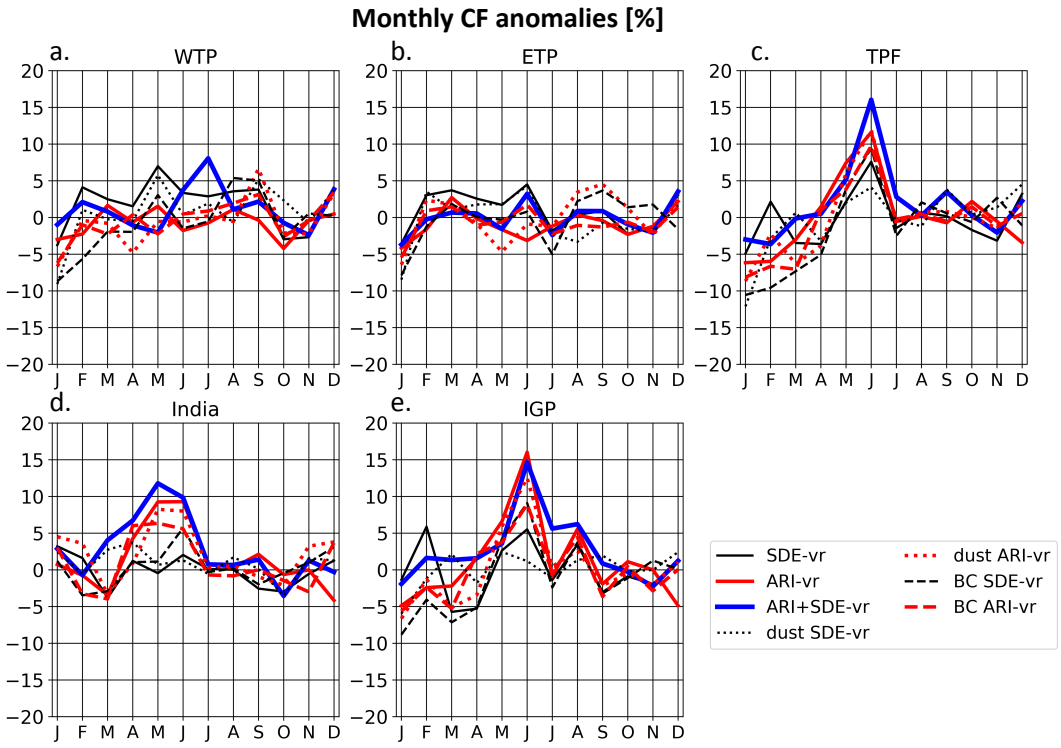

Figure S7. Same as in Figure S4, but for cloud fraction (CF).

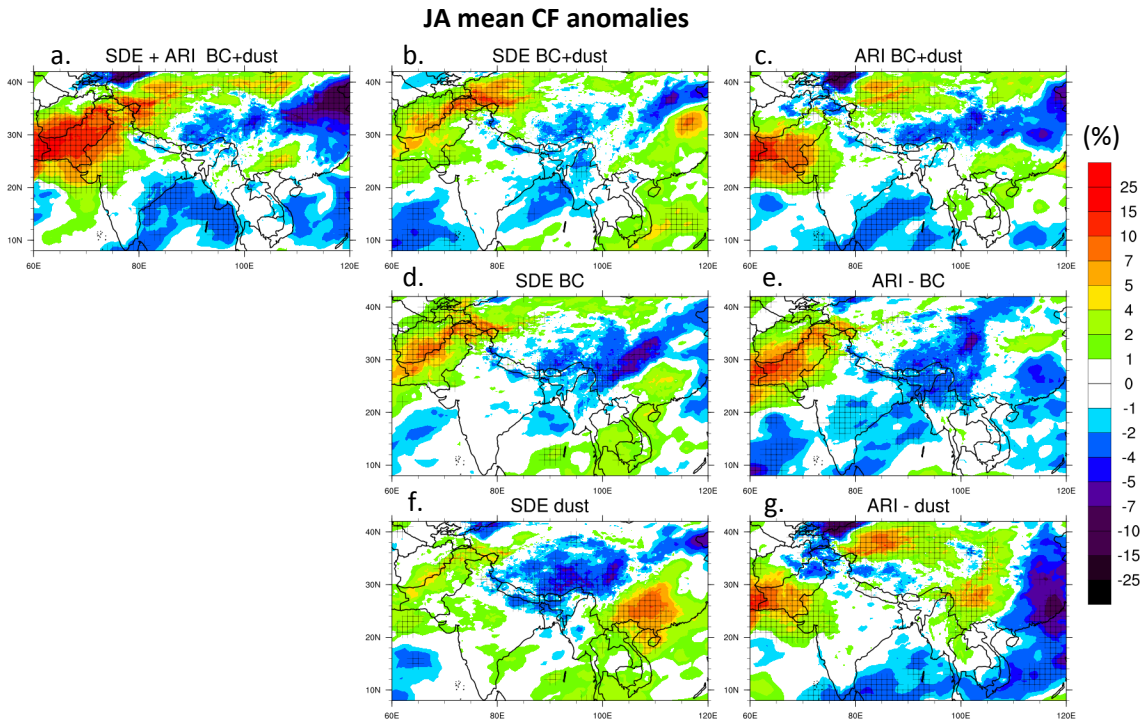

Figure S8. Same as in Figure S3, but for cloud fraction.

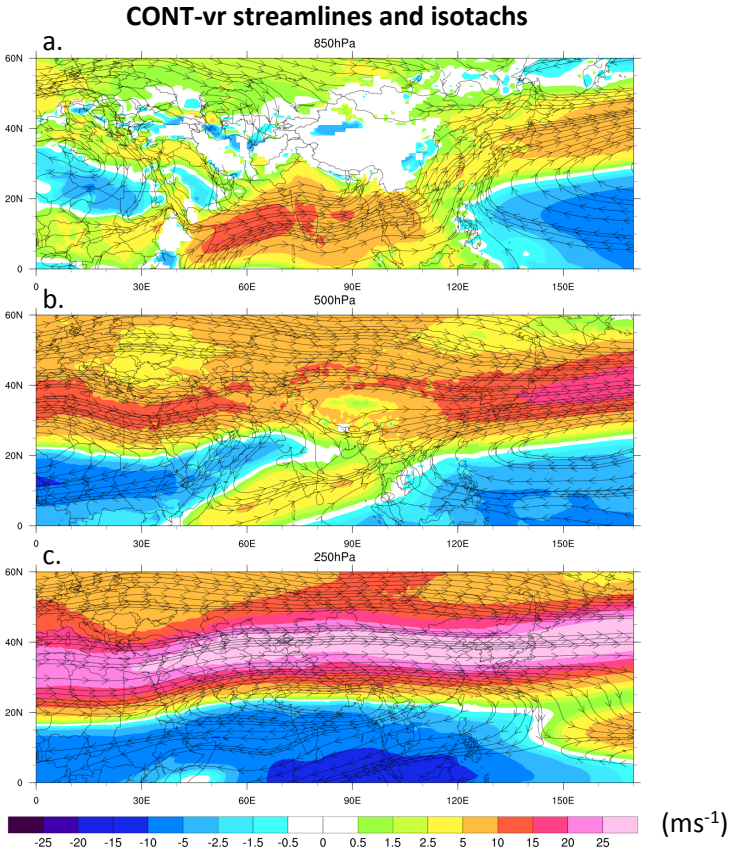

Figure S5. May and June averaged streamlines (black) and *u*-component of the wind (color fill) at (a) 850 hPa, (b) 500 hPa, and (c) 250 hPa in m s^{-1} from CONT-vr.

Stefan Ra
Deleted:

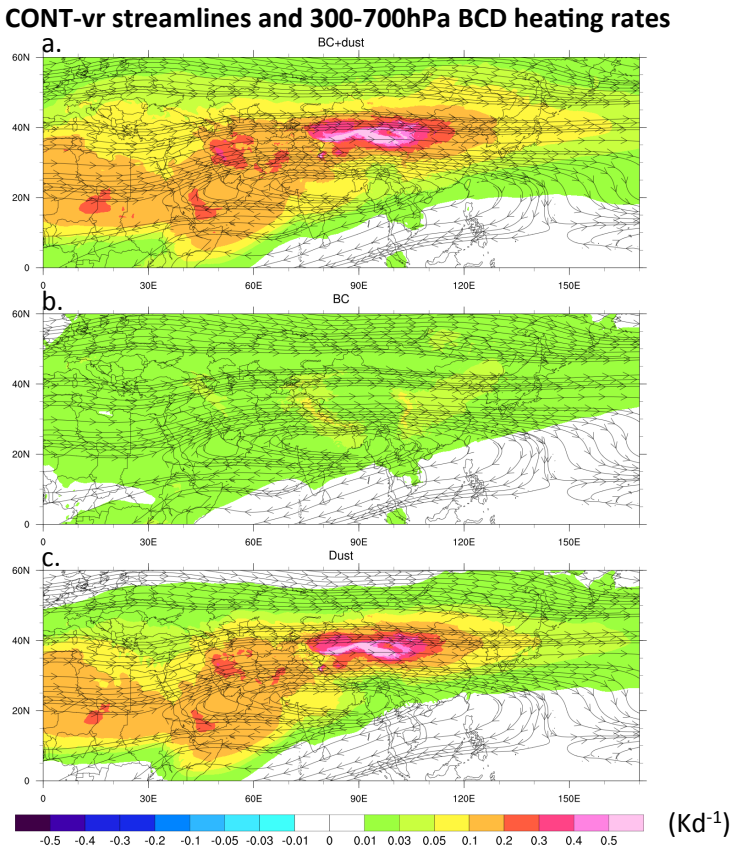

Figure S6. 250 hPa streamlines from CONT-vr and 300-700 hPa column-averaged heating rates due to (a) BCD, (b) BC, and (c) dust.

Stefan Ra
Deleted:

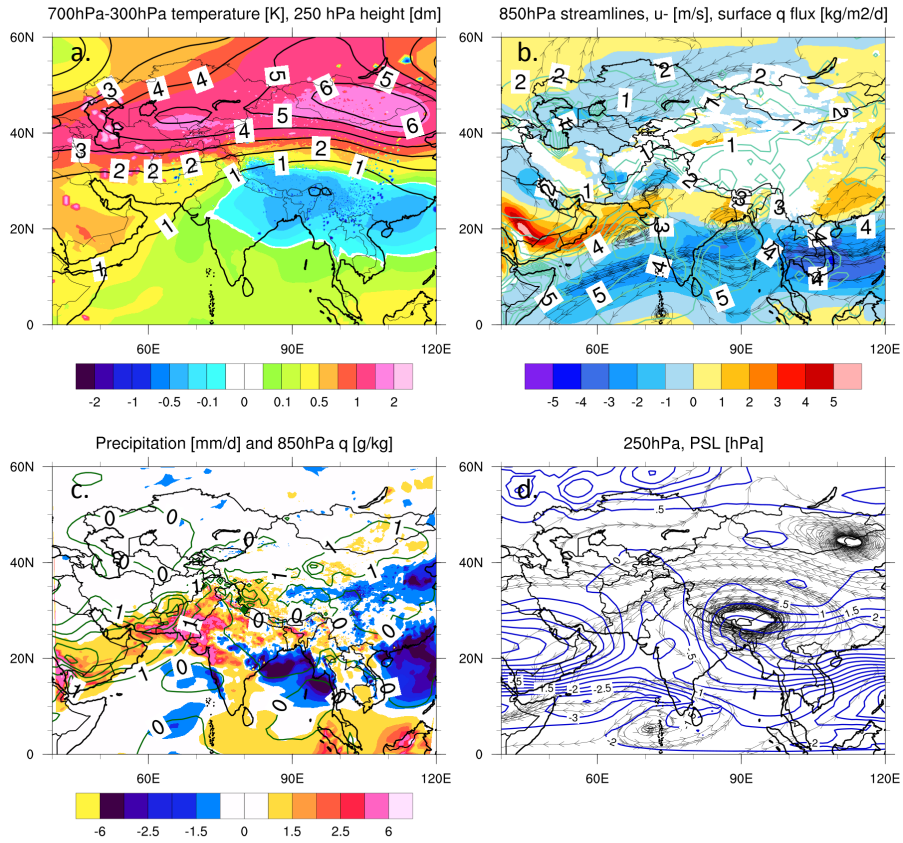

Figure S7. JA averaged BCD-induced anomalies in (a) 700-300 hPa column temperatures and 250 hPa heights, (b) 850 hPa *u*-anomalies (color fill), streamlines, and surface moisture flux (aquamarine contours), (c) precipitation rate (color fill) and 850 hPa specific humidity (dark green contours), and (d) 250 hPa streamlines and surface pressure.

Stefan Ra
Deleted:

References

Kahn Ralph A., Gaitley Barbara J., Garay Michael J., Diner David J., Eck Thomas F., Smirnov Alexander and Holben Brent N.: Multiangle Imaging SpectroRadiometer global aerosol product assessment by comparison with the Aerosol Robotic Network, Journal of Geophysical Research: Atmospheres, 115(D23), doi:10.1029/2010JD014601, 2010.

Levy, R. C., Mattoo, S., Munchak, L. A., Remer, L. A., Sayer, A. M., Patadia, F. and Hsu, N. C.: The Collection 6 MODIS aerosol products over land and ocean, Atmospheric Measurement Techniques; Katlenburg-Lindau, 6(11), 2989, doi:http://dx.doi.org/10.5194/amt-6-2989-2013, 2013.

MISR Science Team: Terra/MISR Level 3, Component Global Aerosol Monthly NetCDF, version 4, Hampton, VA, USA: NASA Atmospheric Science Data Center (ASDC), Accessed 555 AOD from 2002 to 2014 at doi: 10.5067/Terra/MISR/MIL3MAEN_L3.004, 2015

Platnick, S., et al.: MODIS Atmosphere L3 Monthly Product. NASA MODIS Adaptive Processing System, Goddard Space Flight Center, USA: http://dx.doi.org/10.5067/MODIS/MOD08_M3.006, 2015.

Singh, M. K., Gautam, R. and Venkatachalam, P.: A merged aerosol dataset based on MODIS and MISR Aerosol Optical Depth products, in Remote Sensing of the Atmosphere, Clouds, and Precipitation VI, vol. 9876, p. 987627, International Society for Optics and Photonics., 2016.

Smirnov, A., Sayer, A. M., Holben, B. N., Hsu, N. C., Sakerin, S. M., Macke, A., Nelson, N. B., Courcoux, Y., Smyth, T. J., Croot, P., Quinn, P. K., Sciare, J., Gulev, S. K., Piketh, S., Losno, R., Kinne, S. and Radionov, V. F.: Effect of wind speed on aerosol optical depth over remote oceans, based on data from the Maritime Aerosol Network, Atmos. Meas. Tech., 5(2), 377–388, doi:10.5194/amt-5-377-2012, 2012.

Witek, M. L., Diner, D. J., Garay, M. J., Xu, F., Bull, M. A. and Seidel, F. C.: Improving MISR AOD Retrievals With Low-Light-Level Corrections for Veiling Light, IEEE Transactions on Geoscience and Remote Sensing, 56(3), 1251–1268, doi:10.1109/TGRS.2017.2727342, 2018.